Global Contraction of Antarctic Bottom Water between the 1980s and 2000s*

SARAH G. PURKEY AND GREGORY C. JOHNSON

School of Oceanography, University of Washington, and NOAA/Pacific Marine Environmental Laboratory, Seattle, Washington

(Manuscript received 20 October 2011, in final form 19 January 2012)

ABSTRACT

A statistically significant reduction in Antarctic Bottom Water (AABW) volume is quantified between the 1980s and 2000s within the Southern Ocean and along the bottom-most, southern branches of the meridional overturning circulation (MOC). AABW has warmed globally during that time, contributing roughly 10% of the recent total ocean heat uptake. This warming implies a global-scale contraction of AABW. Rates of change in AABW-related circulation are estimated in most of the world's deep-ocean basins by finding average rates of volume loss or gain below cold, deep potential temperature (θ) surfaces using all available repeated hydrographic sections. The Southern Ocean is losing water below $\theta = 0°C$ at a rate of $-8.2\ (\pm 2.6) \times 10^6\ m^3\ s^{-1}$. This bottom water contraction causes a descent of potential isotherms throughout much of the water column until a near-surface recovery, apparently through a southward surge of Circumpolar Deep Water from the north. To the north, smaller losses of bottom waters are seen along three of the four main northward outflow routes of AABW. Volume and heat budgets below deep, cold θ surfaces within the Brazil and Pacific basins are not in steady state. The observed changes in volume and heat of the coldest waters within these basins could be accounted for by small decreases to the volume transport or small increases to θ of their inflows, or fractional increases in deep mixing. The budget calculations and global contraction pattern are consistent with a global-scale slowdown of the bottom, southern limb of the MOC.

1. Introduction

The meridional overturning circulation (MOC) may play a significant role in climate change (e.g., Meehl et al. 2006), and the deep ocean plays a significant role in ocean heat storage (Levitus et al. 2005; Purkey and Johnson 2010). The strength of the MOC determines the ability of the deep ocean to absorb and store anthropogenic heat and carbon (e.g., Sigman and Boyle 2000; Russell et al. 2006). While the MOC has often been considered to be in steady state in recent decades, rates of deep and bottom water production and circulation were dramatically different during the Last Glacial Maximum, and changes in the MOC have been linked to periods of rapid climate change (e.g., Clark et al. 2002; Lynch-Stieglitz et al. 2007). Models suggest the MOC will slow under global warming scenarios, possibly producing large regional variations in surface temperatures (Solomon et al. 2007). Furthermore, climate models differ widely in their projections of how much heat the deep ocean will absorb under global warming, causing a large spread in future climate projections (Boe et al. 2009).

Cold, dense water formed at high latitudes feeds the deep and bottom limbs of the MOC (Lumpkin and Speer 2007). North Atlantic Deep Water (NADW) is a combination of water masses formed in the Labrador and the Nordic seas (LeBel et al. 2008). NADW travels south at depth until it enters the Antarctic Circumpolar Current (ACC) and rises, as seen by the distinct signature of warm, salty water at mid and upper depths (Orsi et al. 1995; Johnson 2008). In the Southern Hemisphere, the densest bottom water, Antarctic Bottom Water (AABW), that underlies NADW is also a mixture of water masses and is formed in at least three locations along the Antarctic continental shelf (Orsi et al. 1999). At each location, physical mechanisms including ice

* Pacific Marine Environmental Laboratory Contribution Number 3771.

Corresponding author address: Sarah G. Purkey, School of Oceanography, Box 357940, University of Washington, Seattle, WA 98195-7940.
E-mail: sarah.purkey@noaa.gov

DOI: 10.1175/JCLI-D-11-00612.1

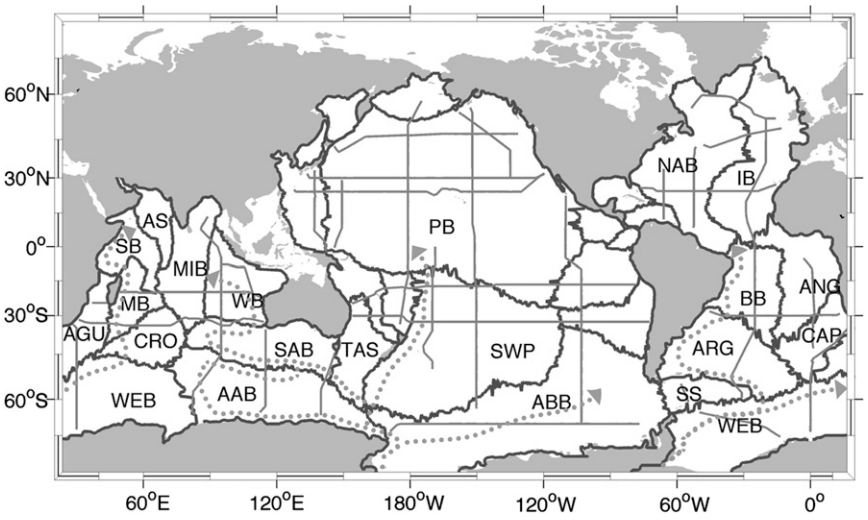

FIG. 1. Basin boundaries (thick black lines), oceanographic sections (thin gray lines), and schematics of the four northward pathways of Antarctic Bottom Water out of the Southern Ocean (dotted gray lines). Key basins are labeled with abbreviations: Agulhas–Mozambique basin (AGU), Crozet basin (CRO), Madagascar basin (MB), Somali basin (SB), Arabian Sea (AS), mid-Indian basin (MIB), Wharton basin (WB), South Australian basin (SAB), Australian–Antarctic basin (AAB), Tasman Sea (TAS), Pacific basin (PB), southwest Pacific basin (SWP), Amundsen–Bellingshausen basin (ABB), Scotia Sea (SS), Weddell–Enderby basin (WEB), Argentine basin (ARG), Brazil basin (BB), North Atlantic basin (NAB), Iberian/Canary/Cape Verde basin (IB), Angola basin (AB), and Cape basin (CAP).

formation, surface cooling, and mixing with ambient water as it cascades down the continental slope (Foster and Carmack 1976) create a distinct variety of AABW. Each AABW variety enters the lower ACC, further mixing with overlying water, and leaves the Southern Ocean as a slightly less dense water mass (Orsi et al. 1999), here still referred to as AABW. AABW flows north, filling the deepest portions of the Pacific, Indian, and western Atlantic oceans (Johnson 2008).

The bottom, southern limb of the MOC transports roughly 20 Sv (1 Sv $\equiv 10^6$ m^3 s^{-1}) northward out of the Southern Ocean (Lumpkin and Speer 2007), primarily in four deep western boundary currents (DWBCs; Fig. 1). Chlorofluorocarbon-11 (CFC-11) inventories confirm that true AABW and other warmer, lighter water masses formed in the Southern Ocean contribute about 21 Sv to this MOC limb (Orsi et al. 2002). Inverse models estimate northward transports of AABW into the Pacific, Atlantic, and Indian Oceans from 7–11, 5–6, and 8–10 Sv, respectively, although definitions of AABW density and the location of the Southern Ocean boundary vary slightly among studies (Ganachaud and Wunsch 2000; Sloyan and Rintoul 2001; Lumpkin and Speer 2007). Velocity measurements within DWBCs along the Kerguelen Plateau in the Indian Ocean and north of the Falkland Plateau in the Atlantic Ocean imply northward transports of ~8 Sv of water for potential temperature $\theta \leq 0.2$°C in each but with high temporal variability (Whitworth et al. 1991; Fukamachi et al. 2010). In the Pacific, velocity measurements at 32°S have shown the DWBC to transport 15.8 (±9.2) Sv of bottom and deep waters, mostly of southern origin, northward (Whitworth et al. 1999).

Numerous studies have shown that the Southern Ocean has warmed significantly throughout the water column. The upper 1000 m of the Southern Ocean has warmed faster than the upper-ocean global mean rate between the 1950s and 2000s (Gille 2002; 2008; Böning et al. 2008). Below 1000 m, the deep ocean has warmed by ~0.03°C decade^{-1} south of the Subantarctic Front between the 1980s and 2000s (Purkey and Johnson 2010). In addition, previous studies have shown property changes in AABW and its components near its source regions. In the Weddell Gyre, Warm Deep Water (WDW), Weddell Sea Deep Water (WSDW), and Weddell Sea Bottom Water (WSBW) have all exhibited warming trends since 1990, although, more recently, WDW has fluctuated between warming and cooling (Robertson et al. 2002; Fahrbach et al. 2004, 2011). In addition, glacier melt has freshened shelf water near the deep-water formation regions in the Weddell Sea (Hellmer et al. 2011). In the Ross Sea, shelf water and bottom water have freshened over the past 50 years (Jacobs and Comiso 1997; Jacobs and Giulivi 2010).

Finally, bottom waters off the Adelie Coast have cooled and freshened on isopycnals between the mid-1990s and mid-2000s (Aoki et al. 2005; Rintoul 2007; Johnson et al. 2008a; Jacobs and Giulivi 2010).

Warming of AABW has also occurred along its spreading paths outside of the Southern Ocean (Purkey and Johnson 2010; Kouketsu et al. 2011). Regional studies within the Scotia Sea, Brazil basin, Argentine basin, Australian–Antarctic basin, Pacific basin, and Southwest Pacific basin have all shown significant warming of AABW over the past few decades (Coles et al. 1996; Fukasawa et al. 2004; Johnson and Doney 2006; Kawano et al. 2006, 2010; Johnson et al. 2007, 2008a; Zenk and Morozov 2007; Meredith et al. 2008). On average, the deep ocean below 4000 m has absorbed $\sim$0.03 W m^{-2} (expressed as a flux over the entire surface area of Earth) between the 1980s and 2000s with stronger warming near the source regions (Purkey and Johnson 2010). The deep-ocean heat uptake, which is often neglected in heat and sea level rise budgets, is important in quantifying earth's net energy imbalance (e.g., Willis et al. 2008; Church et al. 2011). In climate models, periods of decreased upper-ocean heat uptake (and pauses in global average surface warming) are characterized by increases in deep-ocean heat uptake (Meehl et al. 2011), further emphasizing the importance of accurately quantifying total ocean heat uptake, not just the upper few hundred meters.

It is difficult to quantify past effects of global warming on the MOC strength directly owing to a lack of the data needed to determine its historical strength and natural variability (Kanzow et al. 2007). Using data from multiple occupations of a single zonal hydrographic section across the North Atlantic, Bryden et al. (2005) found a 30% reduction in the upper, northern limb of the MOC from 1957 to 2003. However, mooring array data later showed short-term variability to be larger than the previously reported long-term trend from the temporally sparse section data, calling the previous results into question (Cunningham et al. 2007). Using the western halves of most of the occupations of this same section, a decrease in transport in the bottom, southern limb of the MOC carrying AABW northward into the North Atlantic has been reported from 1983 to 2003 (Johnson et al. 2008b), with evidence of a partial rebound in 2010 (Frajka-Williams et al. 2011). While this limb of the MOC may exhibit less temporal variability so far from its source, these transport estimates were still made using geostrophic shear and relying upon an inferred level of no motion. Similarly, a decreasing trend in northward bottom water transport across 24°N in the Pacific has been suggested between 1985 and 2005 (Kouketsu et al. 2009).

However, deep warming signals on pressure surfaces also imply deepening potential isotherms—changes in the vertical distribution of water masses through the water column (Kouketsu et al. 2009, 2011; Masuda et al. 2010). These changes have been attributed to a decrease in bottom water export from the Southern Ocean into deep-ocean basins (Masuda et al. 2010; Kouketsu et al. 2011) and thus could be a signal of a slowdown in the bottom limb of the MOC. Indeed, Kouketsu et al. (2011) found decreases in northward flowing water below 3500 m across 35°S in the Pacific and western Atlantic between the 1990s and 2000s in a data assimilation that includes the deep warming signals.

Here we estimate changes in the bottom, southern limb of the MOC globally using 32 repeated oceanographic sections (hereafter sections), with a total of 145 occupations between 1981 and 2011, by calculating the increase or decrease in volume below multiple deep potential temperature (θ) surfaces. The sections are grouped within and averaged over each measured deep-ocean basin. We use the rates of change in volumes of these cold, dense waters to infer changes in the deep and bottom circulation. While the difference of a section occupied twice may still be subject to short-term variability, the calculation of rates, often over multiple occupations, together with the estimation of means from multiple sections within a basin, usually creates a statistically significant result. This technique allows more robust estimates of changes in the MOC than those derived from geostrophic transport estimates across a single transoceanic hydrographic section.

2. Data

The data used for this study are from an assembly of 32 full-depth, high-quality, and ship-based hydrographic sections that have been occupied two or more times between 1981 and 2011 (Fig. 1). The dataset is comprised of the publicly available conductivity–temperature–depth (CTD) instrument data (available online at http://cchdo.ucsd.edu/) as of September 2011, collected either through the World Ocean Circulation Experiment (WOCE) hydrographic program or the Global Ship-Based Hydrographic Investigations Program (GO-SHIP) in support of the Climate Variability (CLIVAR) and carbon cycle science programs. Data along sections were collected at stations nominally spaced at 55 km. Each station includes a vertical profile of temperature, salinity, and pressure from the surface to a depth of 10–20 m from the bottom. Accuracy of temperature, salinity, and pressure are nominally 0.002°C, 0.002 PSS-78, and 3 dbar, respectively (Joyce 1991). Most of the deep-ocean basins are crossed by at least one section (Fig. 1). The

time and number of occupations varies among sections, but the mean time difference between the first and last occupation for all sections considered here is 14.5 years with the mean first occupation occurring in 1991 and the mean last in 2006. For the three southernmost basins (Fig. 1), the mean time difference is 13.9 years with the mean first occupation in 1993 and the mean last in 2006. Prior to analysis, the data are screened so only data with good quality flags are used. In addition, only occupations deemed sufficiently close (in space) to prior occupations along a given section are used (see Purkey and Johnson 2010 for details).

A full description of the temporal and spatial distribution of the bulk of data used here can be found in Purkey and Johnson (2010). Four new sections and seven new occupations of previously used sections have become available since the publication of Purkey and Johnson (2010) and are added to the dataset they used for this analysis. The new sections, identified by their WOCE designators, include the following: P09 running along 137°E between 10° and 30°N with occupations in 1994 and 2010; S4P running along 67°S between 170°E and 70°W occupied in 1992 and 2011; SR01 running along 65°W between 57° and 63°S occupied in 1993, 1994, 1996, and 1997; and I02/IR06 running roughly along 8°S between 94° and 106°E and then diagonally between 9°S, 106°E and 24°S, 111°E occupied in 1995 and 2000 (Fig. 1). Additional occupations of existing sections previously used include the following: the 1983 occupations of A20 and A22, the 2005 occupation of A12, the 1992 and 2005 occupations of SR04, the 2008 occupation of SR03, and the 2011 partial occupation of A16. All new sections are screened and gridded for use following Purkey and Johnson (2010).

3. Volumetric rate of change analysis

Along many sections, a visible rising or sinking of potential isotherms can be observed between occupations, especially in the Southern Ocean (e.g., Fig. 2). Except within temperature inversions, areas of sinking isotherms are correlated with areas of warming on isobars (and areas of rising with cooling). Similarly, the sinking of an isotherm within a basin implies a loss of water below that θ (Fig. 2), and the rising implies a gain. For example, both occupations of a meridional section across the Australian–Antarctic basin reveal cold AABW cascading down the continental shelf into the deep ocean on the southern side of the basin (Fig. 2a). However, the coldest deep isotherms ($\theta \leq -0.2$°C) across this basin systematically fall with time between occupations, implying a volumetric loss of these deep and bottom waters. By $\theta = 0.2$°C the isotherms are centered around similar depths for both occupations,

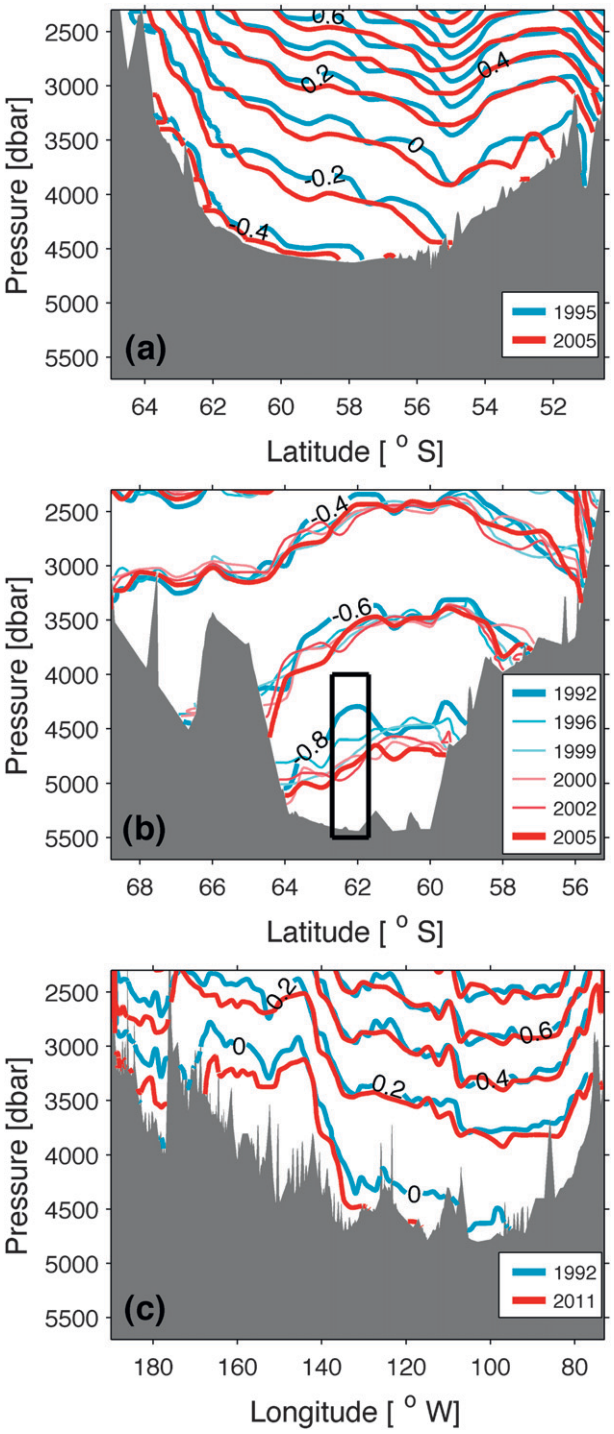

FIG. 2. Vertical–lateral profiles of select potential isotherms for each occupation of (a) I09 across the Australian–Antarctic basin, (b) A12 across the Weddell–Enderby basin, and (c) S4P across the Amundsen–Bellingshausen basin (Figs. 1 and 6). Contours of the earliest occupations are labeled and bottom topography (Smith and Sandwell 1997) is shaded gray. The black box in (b) is discussed in Fig. 3.

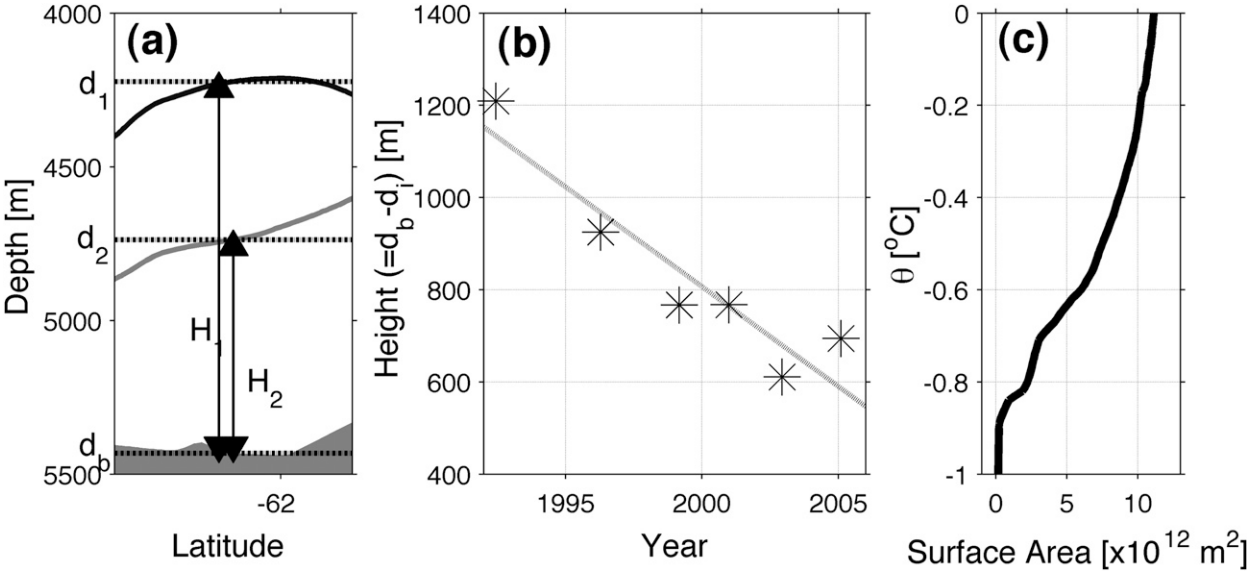

FIG. 3. Illustration of a sample volume contraction calculation taken from A12 in the Weddell–Enderby basin at 62.2°S. (a) Detail of black box in Fig. 2b. Only the depth and thickness for the 1992 (dark gray line and H_1) and 2005 (light gray line and H_2) −0.8°C potential isotherm are shown with bottom topography (Smith and Sandwell 1997) shaded gray. (b) Height of $\theta = -0.8$°C above the bottom (H) at 62.2°S during each occupation (asterisks) with a least squares linear fit (dotted line). (c) Surface area of each given θ in the Weddell–Enderby basin estimated from a climatology (Gouretski and Koltermann 2004).

implying an increase with time in the volume of water within $-0.2° \le \theta \le 0.2$°C that compensates for the contraction of the coldest waters near the bottom, at least in this particular section.

To quantify the loss or gain of water as a function of θ, we first calculate the depth of the isotherms for each occupation along each section. We analyze 811 θ surfaces, referred to as the θ grid, ranging from −2.2° to 32°C with a spacing of 0.01°C below 3°C and a spacing of 0.1°C above 3°C. For each occupation at each location along a section, the θ-pressure profile is converted to a θ-depth profile and linearly interpolated onto the θ grid. Any θ inversions starting from the bottom up are masked over; in other words, the depth of each θ is defined as the deepest depth at which that θ is found. This convention means that upper–water column θ minimums (inversions) are not included in this analysis.

The sections are apportioned to the 33 deep basins they cross. The basin boundaries follow the bottom topography and are mostly isolated by at least the 3000-m isobath (Fig. 1; Smith and Sandwell 1997). The basin boundaries are those used in Purkey and Johnson (2010) except that their Amundsen–Bellingshausen basin (ABB) has been subdivided into the ABB and the Scotia Sea here (Fig. 1). Most of the major deep-ocean basins are crossed by at least one repeat section (Fig. 1), with the exceptions of the Arabian Sea and Somali basin, where no repeat sections are available owing to recent piracy-related safety concerns.

Along each section, within a given basin, the mean rate of change in height above the bottom ($\overline{\partial h/\partial t}$), its standard deviation ($\sigma_{\partial h/\partial t}$), and total degrees of freedom (DOF) are calculated for all values of the θ grid. The height (h) is the difference between the potential isotherm depth (d_i) and that of the sea floor (d_b; Smith and Sandwell 1997; Fig. 3a). The quantity $\partial h/\partial t$ is found from the slope of a least squares linear fit of the isotherm heights to their dates of occupation (e.g., Fig. 3b). The DOF are computed as the horizontal length of the section sampled for $\partial h/\partial t$ for a given isotherm divided by a horizontal decorrelation scale for deep-ocean θ of 163 km estimated by Purkey and Johnson (2010). Sampled regions isolated by topography over a distance less than the decorrelation length scale and separated from adjacent sampled regions by distances more than the decorrelation length scale are assumed to be statistically independent and add one DOF.

Two screening criteria are applied to mask out regions with insufficient spatial or temporal coverage. First, if the time between the first and last occupation is less than 2.5 years, $\partial h/\partial t$ is discarded. Second, if the sum of the area covered by a given θ along a section is less than 111 km, $\overline{\partial h/\partial t}$ is not used. Isotherms sampled for less than 111 km are likely based on data from two or fewer CTD stations, making their mean depth unreliable. This criterion eliminates the coldest, deepest isotherms in many basins (such as the coldest AABW water

cascading down over the Antarctic continental shelf and slope), but it ensures that we are looking at robust, basin-scale means, which are the focus of this paper.

The $\overline{\partial h/\partial t}$, $\sigma_{\partial h/\partial t}$, and DOF along all sections within a given basin are used to compute the basin-mean $\overline{\partial h/\partial t}$, $\overline{\partial h/\partial t}_{\text{bsn}}$, and its uncertainty for each θ value. If there is only one section crossing the basin, the $\overline{\partial h/\partial t}$ for that section is assumed to represent the whole basin. If there are multiple sections crossing a given basin, a length-weighted average is found using the horizontal length occupied by each θ on each section as its weight. The standard error is calculated by dividing the standard deviation by the square root of the DOF, and then a length-weighted average of the standard errors is found. The total DOF for the basin is the sum of the DOF associated with each θ for all sections within the basin. In addition to the basin variability, the 3 dbar and 0.002°C measurement accuracy of the CTD pressure and temperature sensors translate to a 12-m uncertainty at most in isotherm depths for any given cruise. This instrumental uncertainty is neglected hereafter because it is very small compared to that arising from natural variability (e.g., Fig. 2).

Finally, the $\overline{\partial h/\partial t}_{\text{bsn}}$ is scaled to a rate of change in volume (ΔV) within the basin using climatological data (Gouretski and Koltermann 2004; e.g., Fig. 3c). The climatological dataset has a half-degree horizontal resolution with 45 depths. At each location θ is calculated from salinity, temperature, and depth data. Each profile is interpolated onto a 20-m vertical grid using a piecewise cubic Hermite interpolation and linearly interpolated onto the θ grid following the same method described above. The climatological data are divided into the 33 basins. For each basin, the total surface area covered by each θ is calculated. The $\overline{\partial h/\partial t}_{\text{bsn}}$ and associated standard error for each basin are converted to ΔV within that basin by multiplying by the corresponding climatological surface area. Two-sided 95% confidence intervals are estimated from Student's t distribution using the standard errors and total DOF.

The result is a profile of ΔV versus θ with 95% confidence intervals for each of the 27 basins with data (e.g., Fig. 4). Negative values of ΔV indicate a contraction of water below the associated potential isotherm, zero indicates no change, and positive indicates net gain. When water is lost between successively warmer isotherms, the ΔV curves have a negative slope. Vertical portions of the curves indicate no additional loss of water between isotherms, but also no recovery. A positive slope indicates an increase in the amount of water between successively warmer isotherms. The error estimate reflects both the variability across sections and the number of data points. If a given θ is not well sampled, its associated error will be large. The surface area of each isotherm scales both its ΔV and the associated error. For example, the 95% confidence interval around the Weddell-Enderby basin (WEB) ΔV curve (Fig. 4a) narrows with increasing depth (decreasing θ) since the total basin volume below a given isotherm decreases with decreasing temperature. In contrast, the $\overline{\partial h/\partial t}_{\text{bsn}}$ and associated error for the WEB does not (Fig. 5).

4. Southernmost basin changes

The ΔV profiles of the three southernmost basins (Fig. 1) all show a remarkably similar pattern (Fig. 4; orange curves). Each reveals a loss of volume, ranging from -1.6 to -3.6 Sv, within the coldest ~0.5°C of the water column and a recovery from the bottom water contraction within the θ classes of the Circumpolar Deep Water (CDW).

In the WEB (Fig. 1) of the South Atlantic Ocean, a contraction of bottom water is found for $\theta < -0.55$°C, with a maximum value of -3.6 (± 2.0) Sv (Fig. 4a). This rate of change in volume is equivalent to a mean isotherm fall rate of ~15 m yr^{-1} (not shown). Within error bars, this maximum value of ΔV aligns with the -0.7°C boundary between WSBW and WSDW (Carmack and Foster 1975; Orsi et al. 1993) and is found roughly 1000–2000 m above the bottom of the basin. Above the WSBW, we find no significant gain or loss of WSDW for $-0.7° < \theta < 0$°C (Fig. 4a). The bottom water contraction is compensated higher in the water column by an increase in the volume of water with $0.25° < \theta < 0.5$°C. This water is found shallower than 1000 m, where a tongue of lower CDW rises to the south in the ACC as it enters the basin from the north. The ΔV curve for the basin suggests a southward surge of CDW into the region.

Is there a discernible regional pattern of AABW contraction within the WEB? The WEB ΔV curve contains data from three sections: the zonal section SR04 cutting across the Weddell Gyre at approximately 65°S, the meridional section A12 running along the Greenwich Meridian, and the meridional section I06 running along 30°E (Fig. 1). That all three sections show a negative $\partial h/\partial t$ for $\theta < 0$°C and overlap among their 95% confidence intervals indicates an overall consistency of vertical isotherm motions across the basin (Fig. 5). Error is reduced in the mean compared to the individual sections owing to the increase in DOF.

Bumps and wiggles in the mean curves have to be considered in the context of their associated uncertainties. Most sections in the southern basins exhibit a large contraction of water in their coldest temperature class, causing a negative bulge in the mean curve at that

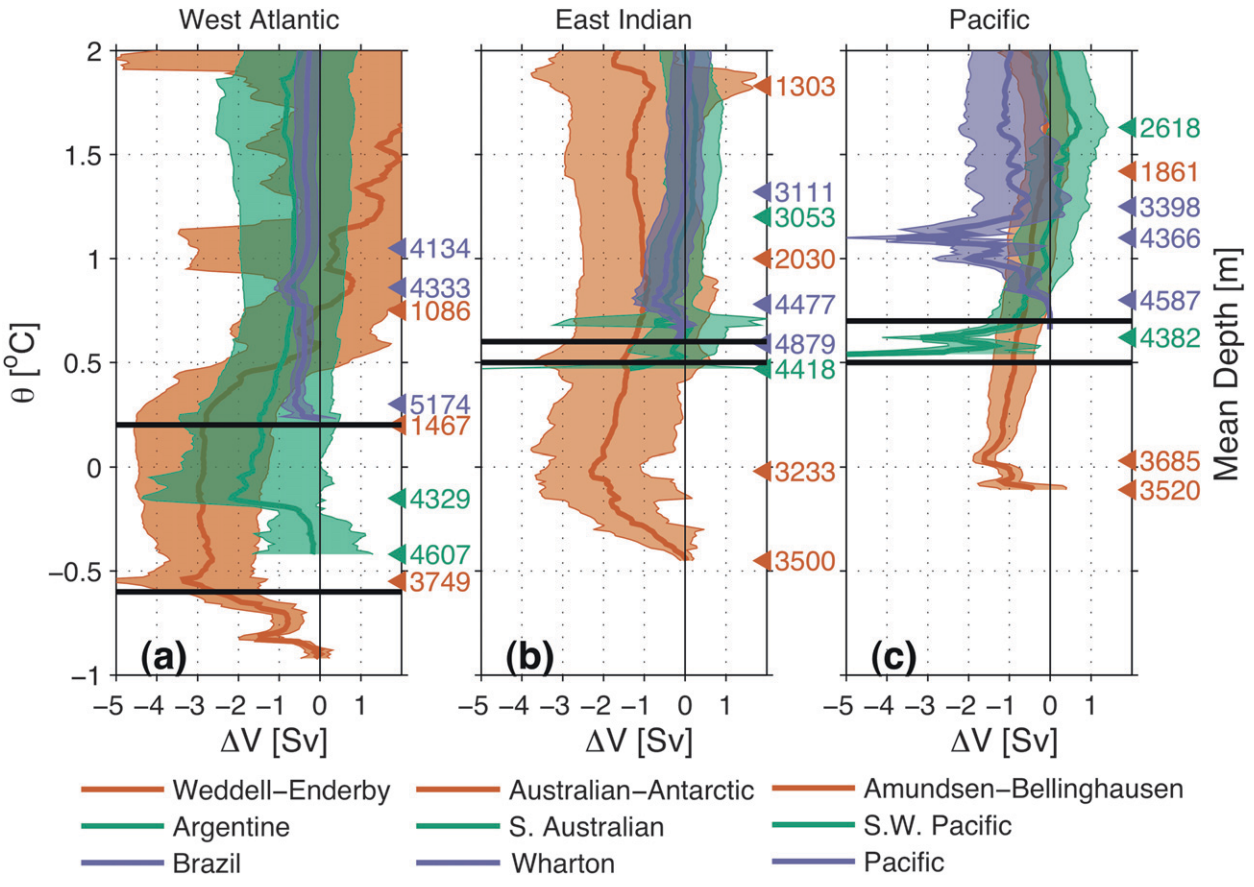

FIG. 4. (a)–(c) Total rates of volume change for select basins (legends) below each potential isotherm (ΔV curves, solid lines) with 95% confidence intervals (shading) along three of the four northward pathways for AABW out of the Southern Ocean from south to north (orange through green to purple). Minimum θ values spreading from the orange to the green basins (lower horizontal black lines) and the green to the purple basins (upper horizontal black lines) are estimated from a climatology (Gouretski and Koltermann 2004). Color-coded numbers along the right axis indicate mean depths of selected θs for the corresponding basin.

potential temperature. The location of the section determines this value, and it does not necessarily represent the overall volume rate of change of the basin. The bulge at $\theta = -0.82$°C in the WEB (Figs. 4 and 5) is an example. This bulge is not outside the confidence limits of the rates given for the θ values above and below (Fig. 4). Thus the θ of maximum volume loss in each basin effectively has uncertainties determined by the confidence intervals for ΔV around that θ. For example, above we assert $\theta = -0.55$°C exhibits maximum volume loss within the WEB. But because the contraction rate at $\theta = -0.55$°C is somewhere between 5.8 and 1.8 Sv, this is only an estimate of the isotherm—at 95% confidence the real value lies somewhere from $0.6° > \theta > -0.7$°C (Fig. 4a).

The Australian–Antarctic basin of the South Indian Ocean (Fig. 1), fed by WSBW, Adelie Land Bottom Water (ALBW; Mantyla and Reid 1995), and Ross Sea Bottom Water (RSBW), shows a loss of -2.2 (± 1.1) Sv of water with $\theta < 0$°C (Fig. 4b), equivalent to a mean isotherm fall rate of 14 m yr^{-1}. The mean ΔV curve does not show a full recovery from the bottom water contraction until $\theta = 2.5$°C, although the curve is not significantly different from zero for $\theta \geq 0.5$°C. These increasing volumes of warmer temperatures suggest a surge of upper CDW from the north is replacing the bottom water losses.

In the ABB of the South Pacific Ocean (Fig. 1), a maximum loss of -1.1 (± 0.3) Sv of water colder than 0°C is found (Fig. 4c), equivalent to a mean fall rate of 13 m yr^{-1}, a pattern similar to that for the Australian–Antarctic basin (Fig. 4b). Water colder than 0°C is within the temperature range of AABW produced in the Ross Sea, RSBW, previously characterized by salinities >34.7 and $\theta < 0$°C (Jacobs et al. 1970). The ABB exhibits a more diffuse recovery from the bottom water contraction than the WEB; in the former the ΔV curve increases slowly between 0 and 1.5°C. Water with $\theta \sim 1.5$°C is upper CDW, found around 1000-m depth in the ABB. Our results suggest an influx of upper CDW from the north in the ABB.

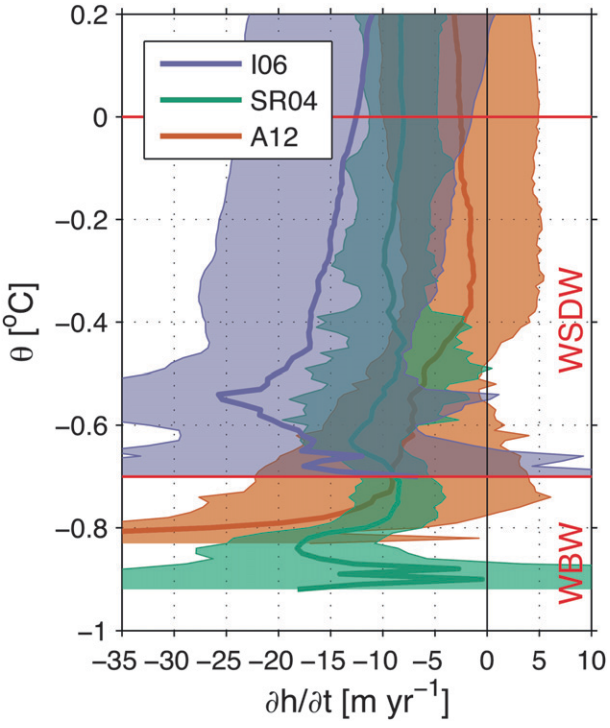

FIG. 5. Mean time rate of change in height above the bottom for potential isotherms along three repeat hydrographic sections across the Weddell–Enderby basin (solid lines; legend; see Fig. 6a for locations) with 95% confidence intervals (shaded). Horizontal red lines indicate classically defined (Carmack and Foster 1975) limits of WSBW ($\theta < -0.7$°C) and WSDW ($-0.7° < \theta < 0$°C).

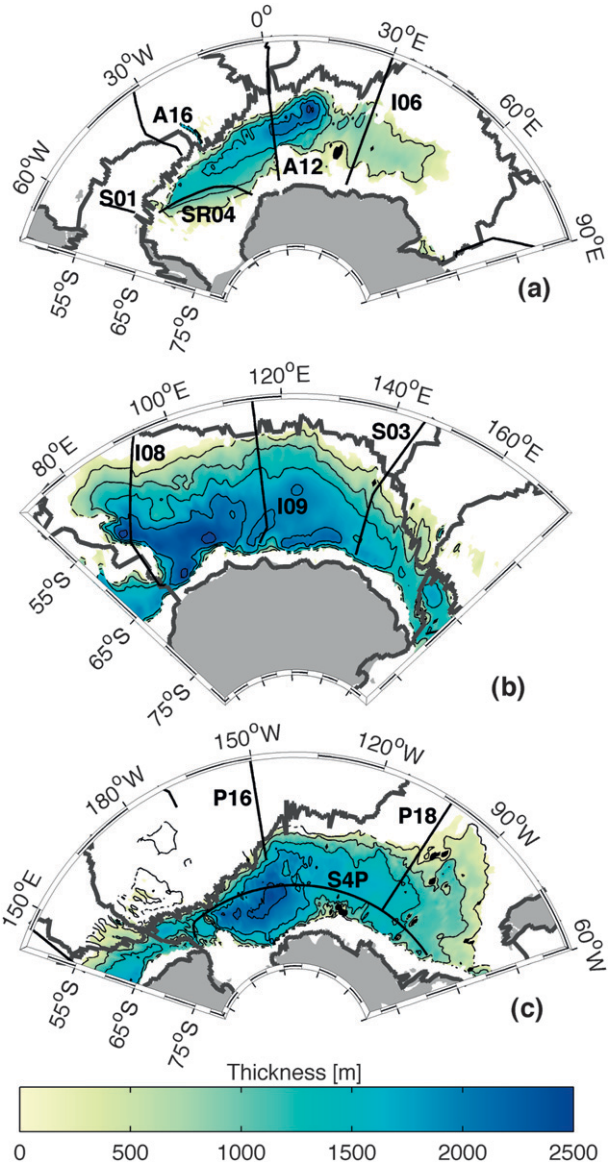

FIG. 6. Thickness (color contours) below select climatological (Gouretski and Koltermann 2004) potential isotherms contained in the southern basins: (a) $\theta = -0.6$°C isotherm in the Weddell–Enderby basin, (b) $\theta = 0.4$°C isotherm in the Australian–Antarctic basin, and (c) $\theta = 0.4$°C isotherm in the Amundsen–Bellingshausen basin. Basin boundaries (thick gray lines), land (shaded gray), and repeat oceanographic sections (black lines) with their WOCE designators are plotted.

5. Changes along the northward paths of AABW

AABW spreads north, primarily along four main DWBCs, out of the Southern Ocean (Fig. 1), filling the bottom-most reaches of most of the world's deep basins (Johnson 2008; Lumpkin and Speer 2007). The Southern Ocean retains a large reservoir of AABW (Fig. 6) as deep ridges restrict its northward transport, their sills limiting the density (and cold temperature) of water that continues north (Orsi et al. 1999; Johnson 2008). The temperature of outflowing waters should be warmed by the observed descent of isotherms in the southern basins, provided they fall at sills. The ΔV curves reveal a clear pattern of decreased AABW volume transport to the north along three of the four main DWBCs leaving the Southern Ocean (Fig. 4). In each case, the θ class below which the contraction is observed increases to the north because of the mixing along the path and, presumably, isotherms sinking with time at the sills.

In the west Atlantic, the basins directly to the north of the WEB along the DWBC of AABW show a volume loss within the AABW (Fig. 4a). Water as cold as $\theta = -0.6$°C leaves the WEB (Fig. 6; Gouretski and Koltermann 2004) and flows into both the Scotia Sea and the Argentine basin (Meredith et al. 2008) although extensive volumes of cold water within these basins do not start until around -0.2°C (Gouretski and Koltermann 2004). In the WEB, a 10 m yr^{-1} isotherm descent rate is observed below -0.2°C. Along the north ridge of the WEB, the vertical θ gradient is about 0.1°C in 300 m, suggesting the outflowing water should have

warmed by roughly 0.07°C over the past ~20 years. This hypothesis is supported by the ΔV curves in the Scotia Sea and Argentine basin to the north.

The Scotia Sea exhibits at most a small and highly uncertain volume loss of −0.4 (±2.1) Sv below 0.2°C. The Scotia Sea is crossed by two meridional sections: A16 and S01. A16 shows a large ~30 m yr^{-1} descent of isotherms between −0.5° and 0.5°C, consistent with the isotherm descent observed in the WEB. However, S01, located farther to the west, shows a rising of isotherms but with an extremely large uncertainty. As a result, the mean (not shown) shows no significant volume loss or gain at any potential temperature. Although no statistically significant trend was found in our analysis, Meredith et al. (2008) reported a decrease in volume of water colder than 0°C in the Scotia Sea between 1995 and 2005 in the A16 data.

Cold water from both the Scotia Sea and directly from the WEB feed the Argentine basin (Fig. 1; Meredith et al. 2008). A maximum bottom water contraction of −2.2 (±2.1) Sv of water below −0.2°C is observed there (Fig. 4a, green curve) equivalent to an isotherm fall rate of ~15 m yr^{-1}, again consistent with observations in the WEB. The first isotherm to span the width of the basin fully is $\theta = -0.2$°C. Between −0.2°C and the coldest sampled water, a small volume loss is observed (Fig. 4). Colder than −0.2°C, isotherms cascade downward on the south side of the basin, and thus only cover a small volume of water. These waters may be undersampled here. We do not quantify volume changes for $\theta < -0.4$°C because there are either no data or insufficient data. A full recovery from the bottom water contraction appears to occur by ~2°, although for $\theta > -0.15$°C the volume changes are no longer significantly different from zero (Fig. 4a). South of the equator, a strong deep thermocline for $1° < \theta < 2$°C denotes the vertical interface between the northward flowing AABW and the southward flowing NADW above (e.g., Johnson and Doney 2006). The ΔV pattern indicates that the AABW contraction may be compensated by an increase in NADW in the Argentine basin.

Farther to the north, in the Brazil basin (Fig. 1), we again find significant loss of the deepest, coldest northward-flowing bottom waters. The coldest water to exit the Argentine basin into the Brazil basin is $\theta \approx 0.2$°C, but again, the bottom of the basin is filled with warmer waters, around 0.3°C. Here, a loss of −0.6 (±0.3) Sv (or a mean isotherm fall rate of 9 m yr^{-1}) for waters colder than 0.3°C is observed in the deepest water. The contraction continues to a maximum loss of −0.8 (±0.3) Sv for waters below 0.86°C (Fig. 4a, purple curve) and does not fully recover until above 2°C, again near the upper extent of AABW influence (e.g., Johnson and Doney 2006).

In the west Indian Ocean DWBC (Fig. 1), bottom water flows out of the WEB into the Crozet basin, followed by the Madagascar basin, Somali basin, and Arabian Sea (e.g., Mantyla and Reid 1995). While this DWBC is fed by the same source water as the northward flowing western Atlantic DWBC, there are no statistically significant cold θ depth changes along this path outside of the WEB, possibly due to a lack of data (Fig. 1). Changes in this DWBC system are not discussed further here.

In the east Indian Ocean, water above 0.5°C flows north out of the Australian–Antarctic basin into the South Australian basin through the Australian–Antarctic Discordance (Fig. 1; e.g., Sloyan 2006). Colder than 0.5°C, a descent rate of −10 (±16) m yr^{-1} is observed in the Australian–Antarctic basin, suggesting about a 0.1°C increase in the coldest bottom water leaving the Australian–Antarctic basin, given the vertical temperature gradient near the basin's northern boundary. The South Australian basin shows a slight loss of ~−0.3 Sv of water colder than 0.7°C, but it is not significantly different from zero (Fig. 4b). Any possible contraction is recovered by 1.2°C and with a continued positive slope the basin shows a net gain in water by 1.7°C. The uncertainties for the ΔV curve in this basin are large, and none of these results are significant at the 95% confidence level.

The Wharton basin (Fig. 1), however, does show a statistically significant loss of bottom water (Fig. 4b). About 4.4–5.8 Sv of water colder than 0.64°C flows out of the South Australian basin into the Wharton basin through a gap between the Broken and Naturaliste plateaus (Sloyan 2006). We find a small but statistically significant contraction of −0.1 (±0.05) Sv below this θ value in the Wharton basin, which shows a maximum decrease of −0.75 (±0.4) Sv at 0.8°C, again corresponding to the coldest waters to span the whole basin. This bottom water contraction slowly recovers between 0.8° and 1.3°C. AABW-derived waters in the Wharton basin cross the mid-Indian ridge into the mid-Indian basin (Warren and Johnson 2002), but we find no significant trend of cold bottom water volumes in the mid-Indian basin (not shown).

In the Pacific, water from both the Australian–Antarctic basin and ABB feed the DWBC that flows northward through the southwest Pacific basin (Fig. 1; Whitworth et al. 1999). The coldest water to enter the southwest Pacific basin has $\theta \sim 0.4$°C, and there is a substantial volume in the basin below 0.6°C. The Australian–Antarctic basin and ABB show an isotherm fall rate between 3 and 6 m yr^{-1} below 0.6°C. Subsequently, the Southwest Pacific basin ΔV profile shows loss of −5 (±4.5) Sv of the coldest measured water at 0.54°C

(Fig. 4c). Above the large bottom water loss, the isotherms between 0.57 and 0.62 all descend by ~12 m yr^{-1}, causing a continued significant contraction rate of ~2 Sv, which is recovered by around 1°C.

The northward flow of bottom water continues into the Pacific basin (Fig. 1) through the Samoan Passage with deep northward flow estimated at 10.6 (±1.7) Sv below $\theta = 1.1$°C and 4.8 (±0.3) Sv below 0.8°C (Roemmich et al. 1996). Here we find a statistically significant reduction of −3.4 (±1.4) Sv below 1.1°C and a small change of ~−0.1 Sv below 0.8°C (Fig. 4c). Above 1.1°C there is a slight recovery, but the curve stays statistically significantly negative, with an isotherm decent of ~0.5 m yr^{-1} until 5°C.

6. Basin budgets

In steady state, maintenance of the vertical θ structure in abyssal basins can be modeled as a balance among the lateral inflow of cold AABW, geothermal heating at the sea floor, vertical mixing with warmer water above, and vertical advection (upwelling). However, the ΔV curves imply that heat and volume budgets below deep, cold θ surfaces are not in steady state in many deep basins. We diagnose these departures from steady state with volume and heat budgets for the Pacific basin below $\theta = 1$°C and the Brazil basin below 0.8°C and determine how inflowing AABW transport or θ, geothermal heating, or vertical mixing would have to change to account for the observed volume and heat changes. We chose these examples because accurate temperature and volume transport estimates are available for these basins below isotherms at which we find significant ΔVs.

Observed ΔV values imply ~15% imbalances in the deep basin volume budgets. Morris et al. (2001) estimate the net lateral inflow of water (through several channels) of $\theta < 0.8$°C into the Brazil basin at 3.70 Sv from current meter data, dominated by a 4.02 Sv inflow through the Vema Channel. Steady-state volume balance would require upwelling at a rate of 3.70 Sv through $\theta = 0.8$°C. However, the observed ΔV of 0.56 Sv at $\theta = 0.80$°C (Fig. 4a) requires a 14% reduction of inflow through the Vema Channel to 3.46 Sv or a 15% increase in upwelling to 4.26 Sv. Similarly, Roemmich et al. (1996) found 11.22 Sv of inflow for $\theta < 1$°C into the Pacific basin through the Samoa Passage and environs. With no lateral outflow of water for $\theta < 1$°C, upwelling through this surface must also be 11.22 Sv in steady state. The observed ΔV of 1.98 Sv at $\theta = 1$°C (Fig. 4c) requires an 18% reduction of inflow or increase of upwelling.

The extent to which the observed ΔV changes perturb the steady-state heat budget can be diagnosed following Morris et al. (2001). By assuming steady-state conservation of volume and heat below cold, deep potential isotherms in the Brazil basin, Morris et al. (2001) estimated vertical diffusion coefficients. We start with a slightly modified steady-state equation (see Table 1) that balances lateral transports and upwelling of heat, vertical mixing of heat, and geothermal heating at the sea floor.

TABLE 1. Heat budget terms (Sv °C) compared to the observed imbalances for two deep basins. (left to right) The advective term is the sum of all cold water volume transports (U_i) through passages i into or out of the basin, each with transport-weighted potential temperatures (θ_i) below a top-bounding potential isotherm (θ_{top}). Upwelling transport through that top surface (W) is derived assuming volume conservation. Values for U_i and θ_i are from Morris et al. (2001) in the Brazil basin and Roemmich et al. (1996) in the Pacific basin. The vertical diffusion term at θ_{top} is the product of the vertical diffusivity coefficient (κ), the vertical temperature gradient (θ_z), and surface area (SA) and is estimated from the residual of the other two steady-state terms. For the geothermal heating term, $Q = 0.05$ W m^{-2}, an average deep-ocean value (Hofmann and Morales Maqueda 2009), is applied over SA, appropriately scaled by density (ρ) and heat capacity (C_p). Climatological maps (Gouretski and Koltermann 2004) are used to estimate θ_z, SA, ρ, and C_p for each basin. The imbalance term (rightmost column) is determined by summing the product of $\partial\Delta V/\partial\theta$ and θ_{top}–θ from the coldest waters in the basin to θ_{top} (see text for further explanation).

	Steady state			
Basin, θ_{top}	$\sum_i U_i\theta_i + W\theta_{top}$	$\kappa\theta_z \times SA$	$\frac{Q \times SA}{\rho C_p}$	$\sum_{\theta}^{\theta_{top}}(\theta_{top}-\theta)\frac{\partial\Delta V}{\partial\theta}$
Pacific basin, 1°C	−2.57	2.38	0.19	−0.15
Brazil basin, 0.8°C	−3.11	3.05	0.06	−0.25

An imbalance term, the rate of change in heat storage (Table 1, rightmost column), is calculated from the ΔV curves (Fig. 4) below select isotherms (θ_{top}). Since the ΔV curves are cumulative sums over θ intervals they are first differentiated with respect to θ, multiplied by θ_{top}–θ (since water must be heated to θ_{top} before exiting the control volume), and then integrated from the bottom up to θ_{top}. In both the Pacific and Brazil basins, the time-dependent heat storage terms are not negligible compared to the dominant terms in the steady-state budget. In the Pacific basin, the heat storage term is ~6% of the advective or mixing terms and comparable to the geothermal term (Table 1). In the Brazil basin, the heat storage term is about 8% of the advective or mixing terms and about four times the magnitude of the geothermal term (Table 1).

We diagnose the changes in water volume transports through deep passages (U_i), transport-weighted potential temperatures of U_i (θ_i), κ, θ_z, or Q (Table 1) required to account for the observed changes in heat storage below θ_{top} in the Brazil and Pacific basins. These

estimates all assume a new steady-state balance has been reached. First, geothermal heating Q would have to almost double in the Pacific basin and more than quintuple in the Brazil basin to account for the observed changes in heat storage. We know of no evidence or plausible reason that such a change in Q has occurred.

In both basin budgets, the heat storage term is about 6% to 8% of the advective and mixing terms. Hence, for the Pacific basin, U_i at the Samoa Passage would have to decrease by 0.65 Sv below 1°C, from 11.22 to 10.57 Sv, to account for the change in heat storage. For the Brazil basin, U_i in the Vema Channel would have to decrease by 0.33 Sv below 0.8°C, from 4.02 to 3.69 Sv. Both changes are less than those required to balance volume. Alternatively, θ_i in the Samoa Passage would have to increase by 0.013°C, from 0.77° to 0.78°C, a plausibly small amount. In the Brazil basin, θ_i through the Vema Channel would have to warm by 0.06°C, from 0.03° to 0.09°C, broadly consistent with an observed 0.03°C decade^{-1} increase in the coldest θ in that channel over recent decades (Zenk and Morozov 2007).

Changes in κ or θ_z required to account for the observed changes in heat storage (Table 1) are equally small. For the Pacific basin κ would have to increase from 5.63 to 5.98 $\times$ 10^{-4} m^2 s^{-1} or θ_z from 0.28 to 0.30 $\times$ 10^{-3} °C m^{-1}. In the Brazil basin, κ would have to increase from 4.34 to 4.70 $\times$ 10^{-4} m^2 s^{-1} or θ_z from 1.41 to 1.53 $\times$ 10^{-3} °C m^{-1} to account for the change in heat storage. Such undetectably small changes cannot be ruled out. However, θ_z increases would be unexpected, since warming bottom waters should decrease θ_z.

7. Discussion

Here we have shown a large decrease of the volume of AABW over time in the Southern Ocean, consistent with a slowdown of the bottom, southern limb of the MOC. Classically defined AABW ($\theta \leq 0$°C) is largely limited to the Australian–Antarctic basin, ABB, WEB, Argentine basin, Scotia Sea, and Agulhas–Mozambique basin. In these basins, $\theta = 0$°C has fallen at a rate of −13.2 (±6.7), −11.4 (±2.9), −8.1 (±4.5), −9.5 (±9.6), −8.6 (±40.3), and −6.4 (±12.1) m yr^{-1}, respectively. The area-scaled sum of these rates yields an estimated contraction rate of −8.2 (±2.6) Sv for water colder than 0°C (Table 2). To the north, along the three best-sampled paths for exporting AABW-derived bottom waters from the Southern Ocean in the lower limb of the MOC, we find a smaller contraction of the volume of the coldest, deepest water. These volume losses suggest a global slowdown of the bottom limb of the MOC. Ventilation time scales along the bottom limb of the MOC from the Southern Ocean to the abyssal North Pacific are of order 1000 years (e.g., DeVries and Primeau 2011), much longer than the time scales of this study. However, previous studies have demonstrated that a reduction of AABW formation around Antarctica can be communicated through the abyss in just decades by planetary waves (e.g., Masuda et al. 2010). Budget calculations in two well-measured deep basins suggest that the observed bottom water temperature trends could be owing to a change in the transport of bottom water entering the basin.

TABLE 2. Rate of volume change below $\theta = 0$°C with 95% confidence intervals (in parentheses) for the six basins containing water this cold (see Fig. 4), and their sum.

Basin	Volume change (Sv)
Weddell–Enderby	−2.85 (±1.59)
Australian–Antarctic	−2.24 (±1.14)
Amundsen–Bellingshausen	−1.09 (±0.28)
Argentine	−1.67 (±1.70)
Scotia Sea	−0.23 (±1.10)
Agulhas–Mozambique	−0.16 (±0.33)
Sum	−8.2 (±2.6)

These results hinge on the assumption that the data analyzed are representative of the deep sampled basins both spatially and temporally over the past few decades. The spatial coverage of the data appears generally good, with most basins analyzed having repeat sections crossing them at roughly even distances, especially in the Southern Ocean (Figs. 1 and 6). This assumption of spatial representativeness can be checked by comparing the isotherm height rates of change ($\partial h/\partial t$) [Eq. (1)] along all sections within basins with multiple crossings. For example, in the WEB, the portions of three sections crossing that basin all show a similar pattern and amplitude in their $\partial h/\partial t$ curves (Fig. 5). On average, isotherms within the WSBW have a descent rate of −22.5 (±21.6) and −11.5 (±13.4) m yr^{-1} along A12 and SR04, respectively (Fig. 5). Within the WSDW, A12, SR04, and I06 exhibit average isotherm descent rates of −3.8 (±7.1), −9.4 (±4.8), and −16.5 (±12.9) m yr^{-1}, respectively (Fig. 5). Given the location of the sections (Figs. 1 and 6) and their relatively uniform patterns of isotherm descents (Fig. 5), it seems unlikely that the volume of the coldest waters has remained constant and instead has shifted around this basin because of changes in gyre strength or location, as suggested previously (Fahrbach et al. 2011). Furthermore, when the ΔV curves for this basin and many others are calculated with different subsamples of the sections crossing those basins, there usually are only small variations in the curves.

Second, here we assume that the temporal data coverage is sufficient to capture any trend. For sections

with more than two occupations, this assumption usually appears valid (e.g., Fig. 2b). Although looking for geostrophic transport trends in multiple occupations of a single section can be misleading because variations in a few stations can dominate such a calculation (e.g., Cunningham et al. 2007), here all the station data from multiple occupations of multiple sections are being averaged over very large areas. This procedure should reduce smaller-scale temporal or spatial noise. Furthermore, our error analysis quantifies the variability within our dataset. In most of the basins presented here, results are statistically significantly different from zero, which suggests that these results are more robust than previous studies of multiple occupations of a single section.

A slowdown of the AABW production rate is consistent with the freshening of shelf waters in AABW formation regions in the Ross and Weddell Seas in recent decades (Aoki et al. 2005; Jacobs and Giulivi 2010; Hellmer et al. 2011). The surface freshening increases the stability of the water column, making it more difficult for surface waters to sink, possibly causing a slowing of the bottom limb of the MOC (Stouffer et al. 2007). In the Ross Sea, the shelf water and RSBW have freshened by ~0.03 and ~0.01 decade^{-1}, respectively, between 1958 and 2008 (Jacobs and Giulivi 2010), most likely caused by recent glacial melt along the Amundsen and Bellingshausen Seas freshening the westward flowing coastal current (Rignot et al. 2008; Jacobs and Giulivi 2010). Along the coast at 140°E and within the central Australian–Antarctic Basin, AABW has also warmed and freshened (Aoki et al. 2005; Johnson et al. 2008a), again pointing toward a freshening of the shelf water end member of either, or both, RSBW and ALBW. In the Weddell Sea, the northwestern shelf water has freshened by 0.09 between 1989 and 2006, owing to increasing glacial meltwater input, changes in sea ice extent, and higher precipitation (Hellmer et al. 2011).

The recent positive trend in the Southern Hemisphere annular mode (SAM) has been connected directly and indirectly to AABW formation rates. Because of past ozone depletion, the summertime SAM index has been trending positive since the 1950s and is predicted to continue positive because of global warming (Thompson et al. 2011). A positive trend in the SAM is associated with stronger and more poleward westerly winds over the Southern Ocean (Gillett and Thompson 2003; Arblaster and Meehl 2006; Thompson et al. 2011) and southward migration of the ACC with associated warming (Gille 2008). Even though the SAM trend is only significant during the summer months and AABW is formed during winter, SAM changes may contribute to increased glacial melt, a southward shift in the ACC, warmer temperatures, and increased precipitation over the Southern Ocean. Given the time scales involved with these phenomena, summer SAM changes could be linked to the observed slowdown of AABW. Further, models have shown the strengthening and the southward migration of westerlies is tied to a net increase of inflow of NADW into the South Atlantic (e.g., Oke and England 2004) and an increase in the northward Ekman transport, which leads to a strengthening of CDW upwelling (e.g., Russell et al. 2006), consistent with our results. Finally, models have also demonstrated that SAM variability can lead to changes in ice formation and melting connected directly to bottom water formation (Gordon et al. 2007; Klinger and Cruz 2009; Kirkman and Bitz 2011).

In addition to a slowdown in AABW formation rates, shifts in other physical processes could also have contributed to the observed AABW volume loss. First, geothermal heating could have increased and warmed AABW. We have no reason to believe geothermal heating in the Southern Ocean has increased dramatically in the past several decades. In more northerly basins, Q would have to increase unrealistically to account for observed heat storage changes (section 6).

Second, one might argue that the same amount of AABW is being produced, but is now warmer and fresher, hence lighter. As noted above, shelf water components of AABW have freshened in recent decades, linked to freshening of ALBW and RSBW (Aoki et al. 2005; Jacobs and Giulivi 2010). In addition, the shelf water entrains adjacent waters as it descends the continental slope to form AABW. Therefore, recently reported warming of adjacent water masses such as CDW (e.g., Böning et al. 2008) or changes in entrainment rates could also affect AABW properties. Indeed, a southward surge of CDW to replace the reduction in AABW, suggested by our calculations, could affect AABW properties. However, if the AABW changes were in its properties and not its formation rate, the ΔV curves in the southernmost basins would exhibit a sharp negative spike centered around the change in θ of the AABW, which is not observed (Fig. 4).

Third, a small change in mixing rates could produce a basin-wide deep warming (e.g., section 6). However, we know of no reason to believe mixing rates have changed over recent decades. Of course, if AABW formation rates have slowed, AABW residence times within these basins could increase, at least while the system adjusts, allowing more time for AABW to mix with overlying waters even if the mixing coefficient does not change. In this respect, the rates of AABW volume changes estimated here can be thought of as an upper

bound on changes in formation rates because mixing may account for some of the changes during any adjustment period.

Here we have suggested that AABW formation has decreased by as much as −8.2 (±2.6) Sv for the period 1993–2006 relative to some previous time period, without addressing the absolute values of AABW formation or when that previous time period might be. How much AABW is being produced presently and how much was produced in the past? While roughly 20 Sv of deep water of Southern Ocean origin has been exported northward in the bottom limb of the MOC in recent decades according to CFC inventories (Orsi et al. 2002) and inverse models (Ganachaud and Wunsch 2000; Sloyan and Rintoul 2001; Lumpkin and Speer 2007), a more relevant formation rate estimate for the classic definition of AABW (roughly $\theta < 0°C$) is 8.1–9.4 Sv from a CFC inventory (Orsi et al. 1999). This inventory-based estimate is centered around 1980 and gives a rough residence time of 120 years using a climatological volume for $\theta < 0°C$ (although the concept of a reference time becomes complex when both the ventilation rate and reservoir volume are changing). If the 8.1–9.4 Sv AABW production rate is representative of earlier decades, our results would seem to imply that AABW production rates have slowed to near zero during the period 1993–2006. Since measurements show AABW is still being produced during these times (e.g., Gordon et al. 2001; Whitworth and Orsi 2006; Williams et al. 2008) this conclusion seems unlikely.

It may be more reasonable to suspect that AABW production rates were already lower around 1980 than in previous decades, so that earlier pure AABW formation could have as much as double the CFC inventory estimate, as supported by the following two arguments. First, a similar NADW formation rate estimate (LeBel et al. 2008) is twice that for pure AABW and about equal for the total contribution of Southern Hemisphere waters to the bottom limb of the MOC, but these southern bottom waters fill about 1.7 times more of the ocean volume than NADW (Johnson 2008), suggesting that over the past millennia or so AABW formation rates may have been on average larger than NADW formation rates. Second, as discussed above, the SAM index has been rising at least since the 1950s and may be associated with a reduction in AABW production rates. Therefore, AABW production rates may have started declining from previous larger values as early as the 1950s.

Acknowledgments. We thank all those who participated in the collection of the WOCE and GO-SHIP data used here. Arnold Gordon made some useful suggestions regarding AABW kinematics. The comments from three anonymous reviewers greatly improved the manuscript. The findings and conclusions in this article are those of the authors and do not necessarily reflect the views of the National Oceanic and Atmospheric Administration (NOAA). This work was supported by the NOAA Climate Program Office, NOAA Research, and NASA Headquarters under the NASA Earth and Space Fellowship Program—Grant NNX11AL89H.

REFERENCES

Aoki, S., S. R. Rintoul, S. Ushio, S. Watanabe, and N. L. Bindoff, 2005: Freshening of the Adélie Land Bottom Water near 140°E. *Geophys. Res. Lett.,* **32,** L23601, doi:10.1029/2005GL024246.

Arblaster, J. M., and G. A. Meehl, 2006: Contributions of external forcings to Southern Annular Mode trends. *J. Climate,* **19,** 2896–2905.

Boe, J., A. Hall, and X. Qu, 2009: Deep ocean heat uptake as a major source of spread in transient climate change simulations. *Geophys. Res. Lett.,* **36,** L22701, doi:10.1029/2009GL040845.

Böning, C. W., A. Dispert, M. Visbeck, S. R. Rintoul, and F. U. Schwarzkopf, 2008: The response of the Antarctic Circumpolar Current to recent climate change. *Nat. Geosci.,* **1,** 864–869.

Bryden, H. L., H. R. Longworth, and S. A. Cunningham, 2005: Slowing of the Atlantic meridional overturning circulation at 25°N. *Nature,* **438,** 655–657, doi:10.1038/nature04385.

Carmack, E. C., and T. D. Foster, 1975: On the flow of water out of the Weddell Sea. *Deep-Sea Res.,* **22,** 711–724.

Church, J. A., and Coauthors, 2011: Revisiting the earth's sea-level and energy budgets from 1961 to 2008. *Geophys. Res. Lett.,* **38,** L18601, doi:10.1029/2011GL048794.

Clark, P., N. G. Pisias, T. F. Stocker, and A. J. Weaver, 2002: The role of the thermohaline circulation in abrupt climate change. *Nature,* **415,** 863–869.

Coles, V. J., M. S. McCartney, D. B. Olson, and W. M. Smethie Jr., 1996: Changes in Antarctic Bottom Water properties in the western South Atlantic in the late 1980s. *J. Geophys. Res.,* **101C,** 8957–8970.

Cunningham, S. A., and Coauthors, 2007: Temporal variability of the Atlantic meridional overturning circulation at 26.5°C. *Science,* **317,** 935–938.

DeVries, T., and F. Primeau, 2011: Dynamically and observationally constrained estimates of water-mass distributions and ages in the global ocean. *J. Phys. Oceanogr.,* **41,** 2381–2401.

Fahrbach, E., M. Hoppema, G. Rohardt, M. Schroder, and A. Wisotzki, 2004: Decadal-scale variations of water mass properties in the deep Weddell Sea. *Ocean Dyn.,* **54,** 77–91.

——, ——, ——, O. Boebel, O. Klatt, and A. Wisotzki, 2011: Warming of deep and abyssal water masses along the Greenwich meridian on decadal time scales: The Weddell gyre as a beat buffer. *Deep-Sea Res. II,* **58,** 2508–2523, doi:10.1016/j.dsr2.2011.06.007.

Foster, T. D., and E. C. Carmack, 1976: Frontal zone mixing and Antarctic Bottom Water formation in the southern Weddell Sea. *Deep-Sea Res.,* **23,** 301–317.

Frajka-Williams, E., S. A. Cunningham, H. Bryden, and B. A. King, 2011: Variability of Antarctic Bottom Water at 24.5°N in the Atlantic. *J. Geophys. Res.,* **116,** C11026, doi:10.1029/2011JC007168.

Fukamachi, Y., S. R. Rintoul, J. A. Church, S. Aoki, S. Sokolov, M. A. Rosenberg, and M. Wakatsuchi, 2010: Strong export of Antarctic Bottom Water east of the Kerguelen plateau. *Nat. Geosci.,* **3,** 327–331, doi:10.1038/ngeo842.

Fukasawa, M., H. Freeland, R. Perkin, T. Watanabe, H. Uchida, and A. Nishima, 2004: Bottom water warming in the North Pacific Ocean. *Nature,* **427,** 825–827.

Ganachaud, A., and C. Wunsch, 2000: Improved estimates of global ocean circulation, heat transport and mixing from hydrographic data. *Nature,* **408,** 453–457, doi:10.1038/35044048.

Gille, S. T., 2002: Warming of the Southern Ocean since the 1950s. *Science,* **295,** 1275–1277.

——, 2008: Decadal-scale temperature trends in the Southern Hemisphere ocean. *J. Climate,* **21,** 4749–4765.

Gillett, N. P., and D. W. J. Thompson, 2003: Simulation of recent Southern Hemisphere climate change. *Science,* **302,** 273–275.

Gordon, A. L., M. Visbeck, and B. Huber, 2001: Export of Weddell Sea deep and bottom water. *J. Geophys. Res.,* **106C,** 9005–9017.

——, ——, and J. C. Comiso, 2007: A possible link between the Weddell Polynya and the Southern Annual Mode. *J. Climate,* **20,** 2558–2571.

Gouretski, V. V., and K. P. Koltermann, 2004: WOCE global hydrographic climatology. Berichte des Bundesamtes für Seeshifffahrt und Hydrographie Rep. 35, 52 pp.+2 CD-ROMs.

Hellmer, H., O. Huhn, D. Gomis, and R. Timmermann, 2011: On the freshening of the northwestern Weddell Sea continental shelf. *Ocean Sci.,* **7,** 305–316, doi:10.5194/os-7-305-2011.

Hofmann, M., and M. A. Morales Maqueda, 2009: Geothermal heat flux and its influence on the oceanic abyssal circulation and radiocarbon distribution. *Geophys. Res. Lett.,* **36,** L03603, doi:10.1029/2008GL036078.

Jacobs, S. S., and J. C. Comiso, 1997: Climate variability in the Amundsen and Bellingshausen seas. *J. Climate,* **10,** 697–709.

——, and C. F. Giulivi, 2010: Large multi-decadal salinity trends near the Pacific–Antarctic continental margin. *J. Climate,* **23,** 4508–4524.

——, A. F. Amos, and P. M. Bruchhausen, 1970: Ross Sea oceanography and Antarctic Bottom Water formation. *Deep-Sea Res.,* **17,** 935–962.

Johnson, G. C., 2008: Quantifying Antarctic Bottom Water and North Atlantic Deep Water volumes. *J. Geophys. Res.,* **113,** C05027, doi:10.1029/2007JC004477.

——, and S. C. Doney, 2006: Recent western South Atlantic bottom water warming. *Geophys. Res. Lett.,* **33,** L14614, doi:10.1029/2006GL026769.

——, S. Mecking, B. M. Sloyan, and S. E. Wijffels, 2007: Recent bottom water warming in the Pacific Ocean. *J. Climate,* **20,** 5365–5375.

——, S. G. Purkey, and J. L. Bullister, 2008a: Warming and freshening in the abyssal southeastern Indian Ocean. *J. Climate,* **21,** 5353–5365.

——, ——, and J. M. Toole, 2008b: Reduced Antarctic meridional overturning circulation reaches the North Atlantic Ocean. *Geophys. Res. Lett.,* **35,** L22601, doi:10.1029/2008GL035619.

Joyce, T. M., 1991: Introduction to the collection of expert reports compiled for the WHP Program. WOCE Hydrographic operations and methods. WOCE operations manual. WHP Office Rep. WHPO-91-1, WOCE Rep. 68/91, 4 pp.

Kanzow, T., and Coauthors, 2007: Observed flow compensation associated with the MOC at 26.5°N in the Atlantic. *Science,* **317,** 938–941.

Kawano, T., M. Fukawasa, S. Kouketsu, H. Uchida, T. Doi, I. Kaneko, M. Aoyama, and W. Schneider, 2006: Bottom water warming along the pathways of lower circumpolar deep water in the Pacific Ocean. *Geophys. Res. Lett.,* **33,** L23613, doi:10.1029/2006GL027933.

——, T. Doi, H. Uchida, S. Kouketsu, M. Fukasawa, Y. Kawai, and K. Katsumata, 2010: Heat content change in the Pacific Ocean between the 1990s and 2000s. *Deep-Sea Res. II,* **57,** 1141–1151, doi:10.1016/j.dsr2.2009.12.003.

Kirkman, C. H., IV, and C. M. Bitz, 2011: The effect of the sea ice freshwater flux on Southern Ocean Temperatures in CCSM3: Deep-ocean warming and delayed surface warming. *J. Climate,* **24,** 2224–2237.

Klinger, B. A., and C. Cruz, 2009: Decadal response of global circulation to Southern Ocean zonal wind stress perturbation. *J. Phys. Oceanogr.,* **39,** 1888–1904.

Kouketsu, S., M. Fukasawa, I. Kaneko, T. Kawano, H. Uchida, T. Doi, M. Aoyama, and K. Murakami, 2009: Changes in water properties and transports along 24°N in the North Pacific between 1985 and 2005. *J. Geophys. Res.,* **114,** C01008, doi:10.1029/2008JC004778.

——, and Coauthors, 2011: Deep ocean heat content changes estimated from observation and reanalysis product and their influence on sea level change. *J. Geophys. Res.,* **116,** C03012, doi:10.1029/2010JC006464.

LeBel, D. A., and Coauthors, 2008: The formation rate of North Atlantic Deep Water and Eighteen Degree Water calculated from CFC-11 inventories observed during WOCE. *Deep-Sea Res. I,* **55,** 891–910.

Levitus, S., J. Antonov, and T. Boyer, 2005: Warming of the world ocean, 1955–2003. *Geophys. Res. Lett.,* **32,** L02604, doi:10.1029/2004GL021592.

Lumpkin, R., and K. Speer, 2007: Global ocean meridional overturning. *J. Phys. Oceanogr.,* **37,** 2550–2562.

Lynch-Stieglitz, J., and Coauthors, 2007: Atlantic meridional overturning circulation during the last glacial maximum. *Science,* **316,** 66–69, doi:10.1126/science.1137127.

Mantyla, A., and J. Reid, 1995: On the origins of deep and bottom waters of the Indian Ocean. *J. Geophys. Res.,* **100** (C2), 2417–2439.

Masuda, S., and Coauthors, 2010: Simulated rapid warming of abyssal North Pacific water. *Science,* **329,** 319–322, doi:10.1126/science.1188703.

Meehl, G. A., and Coauthors, 2006: Climate change projections for the twenty-first century and climate change commitment in the CCSM3. *J. Climate,* **19,** 2597–2616.

——, J. M. Arblaster, J. T. Fasullo, A. Hu, and K. E. Trenberth, 2011: Model-based evidence of deep-ocean heat uptake during surface-temperature hiatus periods. *Nat. Climate Change,* **1,** 360–364, doi:10.1038/NCLIMATE1229.

Meredith, M. P., A. C. Naveira Garabato, A. L. Gordon, and G. C. Johnson, 2008: Evolution of the deep and bottom water of the Scotia Sea, Southern Ocean, during 1995–2005. *J. Climate,* **21,** 3327–3343.

Morris, M., M. M. Hall, L. C. St. Laurent, and N. G. Hogg, 2001: Abyssal mixing in the Brazil Basin. *J. Phys. Oceanogr.,* **31,** 3331–3348.

Oke, R. R., and M. H. England, 2004: Oceanic response to changes in the latitude of the Southern Hemisphere subpolar westerly winds. *J. Climate,* **17,** 1040–1054.

Orsi, A. H., W. D. Nowlin Jr., and T. Whitworth III, 1993: On the circulation and stratification of the Weddell Gyre. *Deep-Sea Res. I,* **40,** 169–203.

——, T. Whitworth III, and W. D. Nowlin Jr., 1995: On the meridional extent and fronts of the Antarctic Circumpolar Current. *Deep-Sea Res. I,* **42,** 641–673.

——, G. C. Johnson, and J. L. Bullister, 1999: Circulation, mixing and production of Antarctic Bottom Water. *Prog. Oceanogr.,* **43,** 55–109.

——, W. M. Smethie Jr., and J. L. Bullister, 2002: On the total input of Antarctic Waters to the deep ocean: A preliminary estimate from chlorofluorocarbon measurements. *Geophys. Res. Lett.,* **107,** 3122, doi:10.1029/2001JC000976.

Purkey, S. G., and G. C. Johnson, 2010: Warming of global abyssal and deep Southern Ocean waters between the 1990s and 2000s: Contributions to global heat and sea level rise budgets. *J. Climate,* **23,** 6336–6351.

Rignot, E., J. L. Bamber, M. R. van Den Broeke, C. Davis, Y. Li, W. Jan Van De Berg, and E. van Meijgaard, 2008: Recent Antarctic ice mass loss from radar interferometry and regional climate modeling. *Nat. Geosci.,* **1,** 106–110, doi:10.1038/ngeo102.

Rintoul, S. R., 2007: Rapid freshening of Antarctic Bottom Water formed in the Indian and Pacific oceans. *Geophys. Res. Lett.,* **34,** L06606, doi:10.1029/2006GL028550.

Robertson, R., M. Visbeck, A. L. Gordon, and E. Fahrbach, 2002: Long-term temperature trends in the deep waters of the Weddell Sea. *Deep-Sea Res. II,* **49,** 4791–4806.

Roemmich, D., S. Hautala, and D. Rudnick, 1996: Northward abyssal transport through the Samoan passage and adjacent regions. *J. Geophys. Res.,* **101C,** 14 039–14 055.

Russell, J. L., D. W. Dixon, A. Gnanadesikan, R. J. Stouffer, and J. R. Toggweiler, 2006: The Southern Hemisphere westerlies in a warming world: Propping open the door to the deep ocean. *J. Climate,* **19,** 6382–6390.

Sigman, D. M., and E. A. Boyle, 2000: Glacial/interglacial variations in atmospheric carbon dioxide. *Nature,* **407,** 859–869.

Sloyan, B. M., 2006: Antarctic bottom and lower circumpolar deep water circulation in the eastern Indian Ocean. *J. Geophys. Res.,* **111,** C02006, doi:10.1029/2005JC003011.

——, and S. R. Rintoul, 2001: The Southern Ocean limb of the global deep overturning circulation. *J. Phys. Oceanogr.,* **31,** 143–173.

Smith, W. H. F., and D. R. Sandwell, 1997: Global seafloor topography from satellite altimetry and ship depth sounding. *Science,* **277,** 1956–1962.

Solomon, S., D. Qin, M. Manning, M. Marquis, K. Averyt, M. M. B. Tignor, H. L. Miller Jr., and Z. Chen, Eds., 2007: *Climate Change 2007: The Physical Science Basis*. Cambridge University Press, 996 pp.

Stouffer, R. J., D. Seidov, and B. J. Haupt, 2007: Climate response to external sources of freshwater: North Atlantic vs. the Southern Ocean. *J. Climate,* **20,** 436–448.

Thompson, D. W. J., S. Solomon, P. J. Kushner, M. H. England, K. M. Grise, and D. J. Karoly, 2011: Signatures of the Antarctic ozone hole in Southern Hemisphere surface climates change. *Nat. Geosci.,* **4,** 741–749, doi:10.1038/NGEO1296.

Warren, B. A., and G. C. Johnson, 2002: The overflows across the Ninetyeast Ridge. *Deep-Sea Res. II,* **49,** 1423–1439, doi:10.1016/S0967-0645(01)00156-4.

Whitworth, T., III, and A. H. Orsi, 2006: Antarctic Bottom Water production and export by tides in the Ross Sea. *Geophys. Res. Lett.,* **33,** L12609, doi:10.1029/2006GL026357.

——, W. D. Nowlin, R. D. Pillsbury, M. I. Moore, and R. F. Weiss, 1991: Observations of the Antarctic Circumpolar Current and deep western boundary current in the southwestern Atlantic. *J. Geophys. Res.,* **96C,** 15 105–15 118.

——, B. A. Warren, W. D. Nowlin Jr., S. B. Rutz, R. D. Pillsbury, and M. I. Moore, 1999: On the deep western-boundary current in the Southwest Pacific basin. *Prog. Oceanogr.,* **43,** 1–54.

Williams, G. D., N. L. Bindoff, S. J. Marsland, and S. R. Rintoul, 2008: Formation and export of dense shelf water from the Adélie Depression, East Antarctica. *J. Geophys. Res.,* **113,** C04039, doi:10.1029/2007JC004346.

Willis, J. K., D. P. Chambers, and R. S. Nerem, 2008: Assessing the globally averaged sea level budget on seasonal to interannual timescales. *J. Geophys. Res.,* **113,** C06015, doi:10.1029/2007JC004517.

Zenk, W., and E. Morozov, 2007: Decadal warming of the coldest Antarctic Bottom Water flow through the Vema Channel. *Geophys. Res. Lett.,* **34,** L14607, doi:10.1029/2007GL030340.